

000
001
002003

Texture Mapping 3D Models of Indoor Environments with Noisy Camera Poses

004
005
006
007
008
009
010
011012 Anonymous 3DIMPVT submission
013014 Paper ID ****
015016

Abstract

Automated 3D modeling of building interiors is useful in applications such as virtual reality and environment mapping. Applying textures to these models is an important step in generating photorealistic visualizations of data collected by modeling systems. Camera pose recovery in such systems often suffers from inaccuracies, resulting in visible discontinuities when different images are projected adjacently onto a plane for texturing. We propose two approaches for reducing discontinuities in texture mapping 3d models made of planar surfaces. The first one is tile based and can be used where camera axes are at arbitrary angles with respect to the plane normals of the surfaces. The second one results in a more seamless texture but is only applicable where camera axes for imagery are closely aligned with plane normals. The effectiveness of our approaches are demonstrated on two indoor datasets.

032

1. Introduction

Three-dimensional modeling of indoor environments has a variety of applications such as training and simulation for disaster management, virtual heritage conservation, and mapping of hazardous sites. Manual construction of these digital models can be time consuming, and as such, automated 3D site modeling has garnered much interest in recent years.

The first step in automated 3D modeling is the physical scanning of the environment's geometry. An indoor modeling system must be able to recover camera poses within an environment while simultaneously reconstructing the 3D structure of the environment itself [2, 6, 7, 8]. This is known as the simultaneous localization and mapping (SLAM) problem, and is generally solved by taking readings from laser range scanners, cameras, and inertial measurement units (IMUs) at multiple locations within the environment.

Mounting such devices on a human-carried platform provides unique advantages over vehicular-based systems on wheels in terms of agility and portability, but can also re-

sult in much larger localization error. As a result, common methods for texture mapping generally produce poor results.

In this paper, we present a number of approaches to texture mapping 3D models of indoor environments made of planar surfaces in the presence of uncertainty and noise in camera poses. In particular, we consider a human-operated backpack system with a number of laser range scanners as well as 2 cameras facing left and right, each equipped with fisheye lenses reaching an approximately 180° field of view. Considering that the human operator walks at about 1 meter/second, and images are captured at 5 Hz, there is a considerable amount of overlap between successive images.

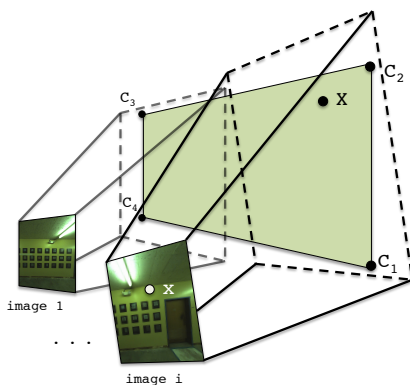
With the laser scanners active, the human operator wearing the backpack takes great care to walk a path such that every wall in the desired indoor environment is traversed and scanned lengthwise at least once.

Using data collected by the onboard sensors and applying multiple localization and loop-closure algorithms [2, 7, 8], the backpack is then localized over its data collection period. This requires recovering the 6 degrees of freedom for the backpack as well as all its sensors, including the cameras mounted on it.¹ Once this is complete, the data from the laser range scanners is used to generate a 3D point cloud of the surrounding environment. Approximate normal vectors for each point in the point cloud are then calculated by gathering neighboring points within a small radius and processing them through principal component analysis. These normal vectors allow for the classification and grouping of adjacent points into structures such as walls, ceilings, floors, and staircases. A RANSAC algorithm is then employed to fit polygonal planes to these structured groupings of points, resulting in a fully planar model [10]. This model, consisting of multiple 2D polygonal planes in 3D space, along with the set of images captured by the backpack's cameras and their noisy 3D poses, can be considered the input to our texture mapping problem.

The remainder of the paper is organized as follows. Section 2 describes the general problem of texture mapping and

¹In this paper, we use the terms localization and pose recovery interchangeably, in that they both refer to recovering position and orientation.

054
055
056
057
058
059
060
061
062
063
064
065
066
067
068
069
070
071
072
073
074
075
076
077
078
079
080
081
082
083
084
085
086
087
088
089
090
091
092
093
094
095
096
097
098
099
100
101
102
103
104
105
106
107

108
109
110
111
112
113
114
115
116
117
118
119
120121 Figure 1: Planes are specified in 3D space by four corners
122 C_1 to C_4 . Images are related to each plane through the cam-
123 era matrices $P_{1..M}$.124
125
126
127
128
129
130
131
132
133
134
135
136
137
138
139
140
141
142
143
144
145
146
147
148
149
150
151
152
153
154
155
156
157
158
159
160
161

examines two variants of a tile-based mapping approach and their shortcomings. Section 3 demonstrates two previous attempts at improving texture alignment, and demonstrates their inadequacies for our datasets. Section 4 presents our proposed approach to texture mapping, combining an improved localization refinement process with two image selection approaches. Section 5 contains results and conclusions.

In all subsequent sections, we discuss the process of texture mapping a single plane, as the texturing of each of our planes is independent and can be completed in parallel.

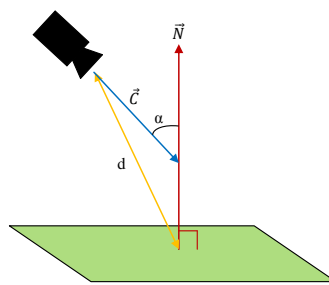
2. Tile-Based Texture Mapping

The geometry of the texture mapping process for a plane is shown in Figure 1. As described earlier, we are provided with a set of M images with which we must texture our target plane. Each image has a camera matrix P_i for $i = 1..M$, which translates a 3D point in the world coordinate system to a 2D point or pixel in image i 's coordinates. A camera matrix P_i is composed of the camera's intrinsic parameters, such as focal length and image center, as well as extrinsic parameters which specify the rotation and translation of the camera's position in 3D world coordinates at the time that image i is taken. These extrinsic parameters are determined by the backpack hardware and localization algorithms [2, 8, 7] and are quite noisy.

Our goal is to texture each plane using images captured by the backpack system, while eliminating any visual discontinuities or seams that would suggest that the plane's texture is not composed of a single continuous image.

2.1. Direct Mapping

Ignoring the fact that the camera matrices $P_{1..M}$ are inaccurate, we can texture the plane by discretizing it into small square tiles, generally about 5 pixels across, and choosing

162
163
164
165
166
167
168
169
170
171
172
173
174
175
176
177
178
179
180
181
182
183
184
185
186
187
188
189
190
191
192
193
194
195
196
197
198
199
200
201
202
203
204
205
206
207
208
209
210
211
212
213
214
215Figure 2: We wish to minimize camera angle α and distance d

an image to texture each tile with. We choose to work with rectangular units to ensure that borders between any two distinct images in our final texture are either horizontal or vertical. Since most environmental features inside buildings are horizontal or vertical, any seams in our texture intersect them minimally and are likely to be less noticeable.

In order to select an image for texturing tile t , we must first gather a list of candidate images that contain all four of its corners, which we can quickly check by projecting t into each image using the projection method above. Furthermore, each candidate image must have been taken at a time when its camera had a clear line-of-sight to t , which can be calculated using standard ray-polygon intersection tests between the camera location, the center of t , and every other plane, all in world coordinates [5].

Once we have a list of candidate images for t , we must define a scoring function in order to compare images and objectively select the best one. Since camera localization errors compound over distance, we wish to minimize the distance between cameras and the plane they texture. Additionally, we desire images that are projected perpendicularly onto the plane, maximizing the resolution and amount of useful texture available in their projections. In other words, we wish to minimize the angle between the plane normal and the camera axis for images selected for texture mapping. These two criteria can be met by maximizing the function $\frac{1}{d}(-1 \cdot \vec{C}) \cdot \vec{N}$ with the parameters shown in Figure 2. Specifically, d is the distance between the centers of a camera and a tile, and \vec{N} and \vec{C} are the directions of the plane's normal and the camera axis respectively.

As Figure 3(a) demonstrates, this approach leads to the best texture for each tile independently, but overall results in many image boundaries with abrupt discontinuities, due to significant misalignment between images, as a result of camera pose inaccuracies.

2.2. Mapping with Caching

Since discontinuities occur where adjacent tiles select non-aligned images that do not align, it makes sense to take into account image selections made by neighboring tiles

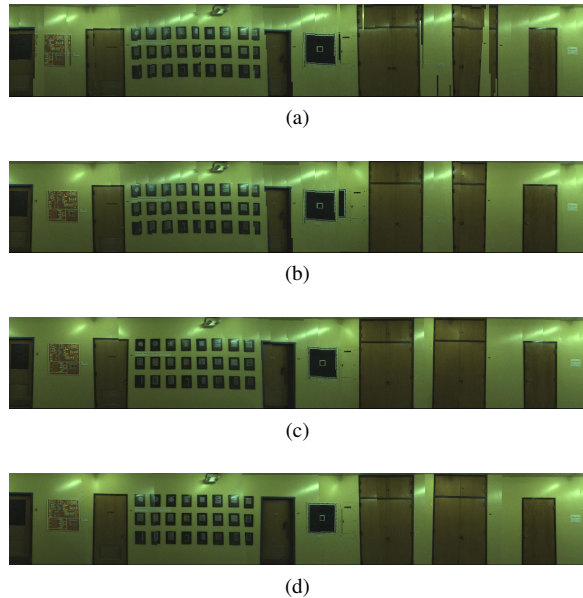


Figure 3: (a): Direct mapping. (b): Mapping with caching. (c): Mapping with caching after image alignment. (d): Seam minimization approach (including image alignment)

while selecting the best image for a given tile. By using the same image across tile boundaries, we can eliminate a discontinuity altogether. If this is not possible because a tile is not visible in images chosen by its neighbors, using similar images is likely to result in less noticeable discontinuities.

Similar to a caching mechanism, we select the best image for a tile t by searching through two subsets of images for a good candidate, before searching through the entire set. The first subset of images is those selected by adjacent tiles that have already been textured. We must first check which images can map to t , and then of those, we make a choice according to the same scoring function. Before reusing this image, we ensure it meets a threshold, which we set unconditionally to $\alpha < 45^\circ$, to be considered a viable image, with α as the camera angle as shown in Figure 2.

If no satisfactory image is found in the first subset, we then check our second subset of images, which consists of images that were taken near the images in the first subset, both spatially and temporally. These images are not the same as the ones used for neighboring tiles, but they were taken at a similar location and time, suggesting that their localization and projection are very similar. Again, if no good image is found according to the same threshold, we must then search the entire set of candidate images, selecting based on the criteria from Figure 2.

The results of this caching approach are shown in Figure 3(b). As compared to Figure 3(a), discontinuities are reduced overall, but the amount of remaining seams sug-

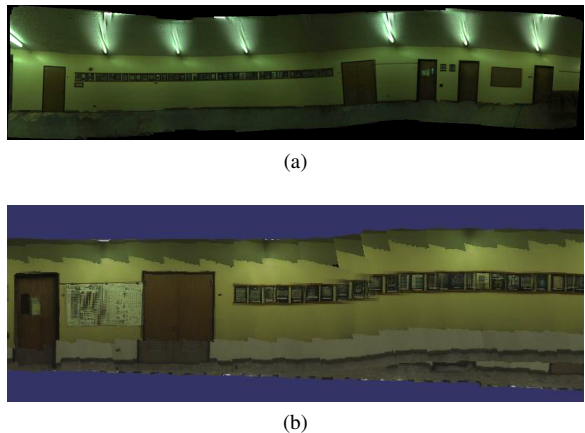


Figure 4: Both image mosaicing (a) and the graph-based localization refinement algorithm from [2] (b) suffer from the problem of compounding errors.

gests that image selection alone cannot produce seamless textures. Camera matrices, or the image projections themselves have to be adjusted in order to reliably generate clean textures.

3. Existing Approaches to Image-Aligned Texture Mapping

In order to produce seamless texture mapping, either camera matrices need to be refined such that their localization is pixel accurate, or image stitching techniques need to be applied to provide this illusion.

Before examining these approaches, we first obtain a set of images to work with. Rather than perform camera or image adjustments across the many thousands of images acquired in a typical data collection, we opt to work with the more limited set of images corresponding to those chosen by the direct mapping approach, without caching (Section 2.1). This set of images constitutes a good candidate set for generating a final seamless texture since it meets three important criteria. First, each tile on our planeis covered by at least one image in this set; this ensures no holes in our final texture. Second, images are all selected according to the scoring function in Figure 2, ensuring good camera distances and angles. Third, as a side result of the scoring function, selected images are only viable candidates for the tiles near their center of projection. Thus, there should be plenty of overlap between selected images, allowing for some degree of shifting without resulting in holes, as well as area for blending between them. With this set of images, we now review two existing approaches towards refining and combining their projections.

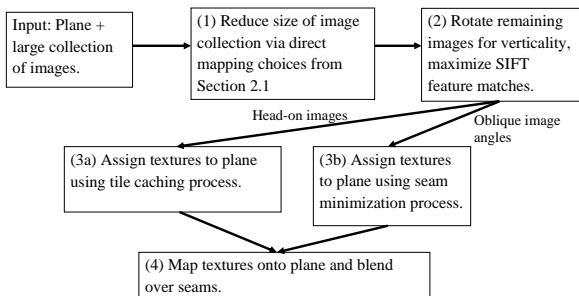


Figure 5: Our proposed method for seamless texture mapping.

3.1. Image Mosaicing

When images of a plane are taken from arbitrary overlapping positions, they are related by homography [6]. Thus, existing homography-based image mosaicing algorithms are applicable [1]. However, errors can compound when long chains of images are mosaiced together using these approaches. For example, a pixel in the n th image in the chain must be translated into the first image's coordinates by multiplying by the 3×3 matrix $H_1 H_2 H_3 \dots H_n$. Any error in one of these homography matrices is propagated to all further images until the chain is broken. For some chains of images this can happen almost immediately due to erroneous correspondence matches and the resulting image mosaic is grossly misshapen.

Figure 4(a) shows the output of the AutoStitch software package which does homography-based image mosaicing. This plane is nearly a best-case scenario with many features spread uniformly across it. Even so, the mosaicing produces errors that cause straight lines to appear as waves on the plane, despite the fact that it was generated after careful hand tuning. Many planes with fewer features simply failed outright. Thus, image mosaicing is not a robust enough solution for reliably texture mapping our dataset.

3.2. Image-Based 3D Localization Refinement

Another approach is to refine the camera matrices using image correspondences to guide the process. Each image's camera matrix has 6 degrees of freedom that can be adjusted. Previous work on this problem attempted to refine camera matrices by solving a non-linear optimization problem [8]. This process is specific to the backpack system which generated our dataset, as it must be run during backpack localization [8, 2]. This approach suffers from a similar error propagation problem as shown in Figure 4(b).

4. Proposed Method for Seamless Texture Mapping

In this section, we will describe our proposed method for seamless texture mapping. Our approach consists of 4 steps, as seen in Figure 5. First, we choose a subset of M images to work with via the direct mapping approach of Section 2.1. Next, we perform image rotation and shifting in order to maximize SIFT feature matches in overlapping areas between images. We then project these images onto our plane, applying textures either with the tile caching method from Section 2.2, or with the more specialized method to be described in Section 4.3. This choice depends on the availability of head-on images for a given plane. We then finish by applying linear alpha blending to smooth out any remaining seams.

4.1. Image Projection and Rotation

We begin with the projection of all images onto the plane. This is done in the same way as the approaches in Section 2. We then perform rotations on these projections, as adjacent images with different orientations result in strong discontinuities.

These rotations are accomplished by using Hough transforms, which detect the presence and orientation of linear features in our images. Rather than match the orientation of such features in each image, we simply apply rotations such that the strongest near-vertical features are made completely vertical. This is effective for vertical planes in indoor models, since they usually consist of parallel vertical lines corresponding to doors, wall panels, rectangular frames, etc. If features in the environment are not vertical, or are not parallel to each other, this step is skipped.

4.2. Image Pose Refinement

Our next step is to align overlapping images by searching for corresponding points between all pairs of overlapping images using SIFT feature matching [9]. The SIFT matches determine dx and dy distances between each pair of features for two images on the plane, though these distances may not always be the same for different features.

Since indoor environments often contain repetitive features such as floor tiles or doors, we need to ensure that our SIFT-based distances are reliable. In order to mitigate the effect of incorrect matches and outliers, the RANSAC framework [4] is used for a robust estimate of the optimal dx and dy distances between two images. The RANSAC framework handles the consensus-building machinery, and requires a fitting function and a distance function. For this application, the fitting function simply finds the average distance between matches in a pair of images. Our distance function for a pair of points is the difference between those points' SIFT match distance and the average distance

324	378
325	379
326	380
327	381
328	382
329	383
330	384
331	385
332	386
333	387
334	388
335	389
336	390
337	391
338	392
339	393
340	394
341	395
342	396
343	397
344	398
345	399
346	400
347	401
348	402
349	403
350	404
351	405
352	406
353	407
354	408
355	409
356	410
357	411
358	412
359	413
360	414
361	415
362	416
363	417
364	418
365	419
366	420
367	421
368	422
369	423
370	424
371	425
372	426
373	427
374	428
375	429
376	430
377	431

432 computed by the fitting function; we use a 10 pixel outlier
 433 threshold. This means that a SIFT match is labeled as an
 434 outlier if its horizontal or vertical distance is not within 10
 435 pixels of the average distance computed by the fitting func-
 436 tion.
 437

438 439 4.2.1 Refining Image Positions using Least Squares

440 There are a total of M^2 possible pairs of images, though
 441 we only generate distances between images that overlap at
 442 SIFT feature points. Given these distances and the origi-
 443 nal image location estimates, we can solve a least squares
 444 problem ($\min_{\vec{\beta}} \|X\vec{\beta} - \vec{\gamma}\|_2^2$) to estimate the correct location
 445 of the images on the plane. The M -dimensional vector $\vec{\beta}$
 446 represents the unknown x and y locations of each image on
 447 the plane from $1 \dots M$. The optimal x and y locations are
 448 obtained in the same way, so we only consider the x loca-
 449 tions here:
 450

$$452 \vec{\beta} = (x_1, x_2, x_3, \dots x_{M-1}, x_M)$$

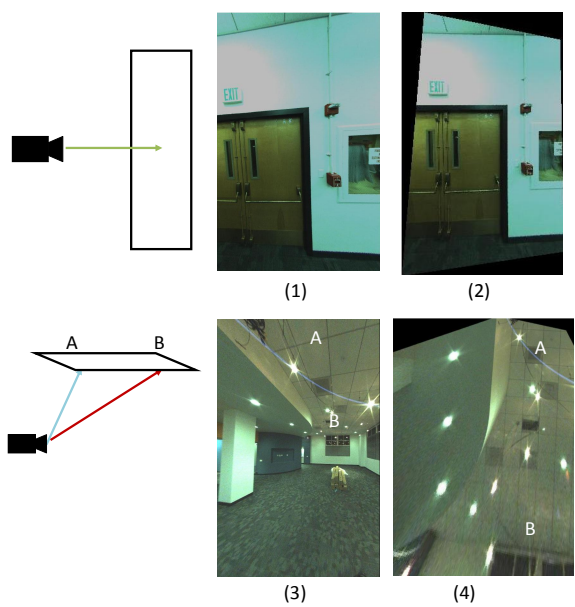
453 The N by $(M + 1)$ dimensional matrix X is constructed
 454 with one row for each pair of images with measured dis-
 455 tances produced by the SIFT matching stage. A row in the
 456 matrix has a -1 and 1 in the columns corresponding to the
 457 two images in the pair. For example, the matrix below in-
 458 dicates that we generated a SIFT-based distance between
 459 images 1 and 2, images 1 and 3, images 2 and 3, etc.
 460

$$461 X = \begin{pmatrix} -1 & 1 & 0 & \dots & 0 & 0 \\ -1 & 0 & 1 & \dots & 0 & 0 \\ 0 & -1 & 1 & \dots & 0 & 0 \\ \vdots & \vdots & \vdots & \ddots & \vdots & \vdots \\ 0 & 0 & 0 & \dots & 1 & 0 \\ 0 & 0 & 0 & \dots & -1 & 1 \\ 1 & 0 & 0 & \dots & 0 & 0 \end{pmatrix}$$

470 If only relative distances between images are included
 471 then there is no way to determine the absolute location of
 472 any of the images and the matrix becomes rank deficient.
 473 To fix this we choose the first image to serve as the anchor
 474 for the rest, meaning all the absolute distances are based on
 475 its original location. This is done by adding a row with a 1
 476 in the first column and the rest zeros.
 477

478 Finally, the N -dimensional observation vector $\vec{\gamma}$ is con-
 479 structed using the SIFT-based distances generated earlier in
 480 the matching stage. The distances are denoted as $d_1 \dots d_N$
 481 for N SIFT-based distances. The last element in the obser-
 482 vation vector is the location of the first image determined
 483 by its original noisy localization, from [2, 8]:
 484

$$485 \vec{\gamma}^T = (d_{1,2}, d_{1,3}, d_{2,3}, \dots d_{N-2,N-1}, d_{N-1,N}, x_1)$$



505
 506 Figure 6: (1) projects perpendicularly onto a wall and
 507 provides uniformly high resolution textures over its entire pro-
 508 jection (2). (3) on the other hand projects at a poor angle
 509 onto the ceiling (4), resulting in usable texture at point A,
 510 but increasingly low resolution texture towards point B.

511 The $\vec{\beta}$ that minimizes $\|X\vec{\beta} - \vec{\gamma}\|_2^2$ results in a set of image
 512 locations on the plane that best honors all the SIFT-based
 513 distance measurements between images. In practice there
 514 are often cases where there is a break in the chain of im-
 515 ages, meaning that no SIFT matches were found between
 516 one segment of the plane and another. In this case we add
 517 rows to the X matrix and observations to the $\vec{\gamma}$ vector that
 518 contain the original noisy x and y distance estimates gen-
 519 erated by the localization algorithm [2, 8]. Another way to
 520 do this is to add rows for all neighboring pairs of images
 521 and solve a weighted least squares problem where the SIFT
 522 distances are given a higher weight i.e. 1, and the noisy
 523 distances generated by the localization algorithm [2, 8] are
 524 given a smaller weight i.e. 0.01.
 525

526 After completing this same process for the y dimension
 527 as well, and making the resultant shifts, our images over-
 528 lap and match each other with far greater accuracy. Ap-
 529 plying the tile caching method from Section 2.2 on these
 530 re-localized images results in the significant improvements
 531 shown in Figure 3(c), as compared to Figure 3(d).
 532

533 4.3. Texture Mapping with Seam Minimization

535 As mentioned earlier, our backpack system has 2 cam-
 536 eras with 180° fisheye lenses facing to the right and left.
 537 Since the backpack operator only takes care to fully scan
 538 each wall and not necessarily the entirety of each ceiling
 539 and floor, cameras at higher angles with respect to plane

540
 541
 542
 543
 544
 545
 546
 547
 548
 549
 550
 551
 normal vectors must be used for texturing large areas of
 floor and ceiling planes. These high camera angles translate
 into images that span extremely large areas once projected.
 Such image projections have good scores (from Figure 2)
 for certain areas on the plane, but much worse scores for
 other areas. This can be seen in Figure 6. The tiling approach
 used in Section 2 was thus a good choice for texturing,
 as it allowed us to only use the parts of image projections
 that were good choices for their respective plane
 locations, e.g. areas near point A in Figure 6, but not near
 point B.

552
 553
 554
 555
 556
 557
 558
 For wall planes however, we have images all taken from
 close distances and more head-on angles, and thus higher
 resolution, near-rectangular projections to work with. As
 a result, there is less deviation over the score of each tile
 within an image, as well as over the average scores of all
 images. This means that the scoring criteria from Figure 2
 is less relevant to walls, which enjoy an abundance of head-
 on images.

559
 560
 561
 562
 563
 564
 565
 Thus, for planes with optimal images, rather than selecting
 the set of best images, since all images are near in quality,
 we instead select the best set of images, such that the
 selection together results in the cleanest final texture. We
 will accomplish this by using entire images where possible,
 and defining a cost function to minimize the visibility of
 seams in our final texture.

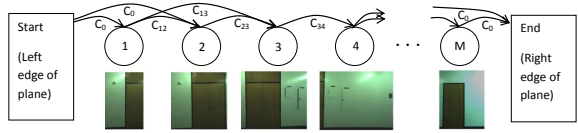
567 4.3.1 Occlusion Masking

568
 569 To begin with, we need to ensure that our images contain
 570 only content that should be mapped onto the target plane in
 571 question. The tiling approach used previously only checks
 572 occlusion for each tile as it is being textured. For our new
 573 approach, we prefer entire images, so we need to perform
 574 occlusion checks over the entirety of each image to determine
 575 available areas for texture mapping.

576 Fortunately, by virtue of our indoor environments, the
 577 vast majority of surface geometry is either horizontal or vertical,
 578 with high amounts of right angles. This means that after
 579 masking out occluded areas, our image projections will
 580 remain largely rectangular. We can thus be efficient by re-
 581 cursively splitting each image into rectangular pieces, and
 582 performing the same occlusion checks used in the tiling pro-
 583 cess where needed. To actually occlude out rectangles, we
 584 simply remove their texture, as we will ensure that untextured
 585 areas are never chosen for texture mapping.

587 4.3.2 Image Selection

588
 589 To determine the set of images that results in the cleanest
 590 texture, we need a cost function to evaluate the visibility
 591 of seams between images in our set. A straightforward
 592 cost function that accomplishes this is the sum of squared
 593 pixel differences in overlapping regions between all pairs



594
 595
 596
 597
 598
 599
 Figure 7: DAG construction for the image selection process.

600
 601
 602
 603
 604
 605
 606
 of images, after they have been aligned as described in Sec-
 607 tion 4.1. Minimizing this cost function encourages image
 608 boundaries to occur either in featureless areas, such as bare
 609 walls, or in areas where images match extremely well.

610
 611
 612
 613
 614
 615
 616
 617
 618
 619
 620
 621
 622
 623
 624
 625
 626
 627
 With the cost function defined, we must now select the
 628 set of images for which the overall cost function is mini-
 629 mized. Since nearly all the images for these optimal cases
 630 are head on, the best strategy to minimize seams is to choose
 631 as few images as possible while texturing a given plane.
 632 Thus, to cover the entirety of a plane, our problem can be de-
 633 fined as minimally covering a polygon i.e. the plane, using
 634 other polygons of arbitrary geometry i.e. our image pro-
 635 jections, with the added constraint of minimizing our cost
 636 function between chosen images. This is a complex prob-
 637 lem, though we can take a number of steps to simplify it.
 638 Given that our wall-texture candidate images are all taken
 639 from a head-on angle, and assuming only minor rotations
 640 are made during localization refinement, we can reason that
 641 their projections onto the plane are approximately rectangu-
 642 lar, as in Figure 6. By cropping them all to be rectangular,
 643 our problem becomes the conceptually simpler one of fill-
 644 ing a polygon with rectangles, such that the sum of all edge
 645 costs between each pair of rectangles is minimal. We thus
 646 also retain the advantages of working with rectangular units,
 647 as explained in Section 2.

648
 649 The location and orientation of the cameras on our back-
 650 pack is such that our images nearly always contain the
 651 entirety of the floor to ceiling range of wall planes. Images
 652 are therefore rarely projected with one above another when
 653 texturing wall planes, which correspond to the optimal case
 654 we are working with. In essence, we need only to ensure
 655 horizontal coverage of our planes, as our images provide
 656 full vertical coverage themselves. We can thus construct a
 657 Directed Acyclic Graph (DAG) from the images, with edge
 658 costs defined by our cost function above, and solve a simple
 659 shortest path problem to find an optimal subset of images
 660 with regard to the cost functions [3].

661
 662 Figure 7 demonstrates the construction of a DAG from
 663 overlapping images of a long hallway. Images are sorted
 664 by horizontal location left to right, and become nodes in a
 665 graph. Directed edges are placed in the graph from left to
 666 right between images that overlap. The weights of these
 667 edges are determined by the cost functions discussed pre-
 668 viously. Next, we add two artificial nodes, one start node
 669 representing the left border of the plane, and one end node

648
649
650
651
652
653
654
655
representing the right border of the plane. The left(right) artificial node has directed edges with equal cost C_0 to(from)
all images that meet the left(right) border of the plane.

656
657
658
659
660
661
662
663
664
665
666
667
668
669
670
We now solve the shortest path problem from the start node to the end node. This provides a set of images completely covering the plane horizontally, while minimizing the cost of seams between images.

671
672
673
674
675
676
677
678
679
In rare cases where the vertical dimension of the plane is not entirely covered by one or more chosen images, we are left with holes where no images are selected to texture. To address this, we simply modify the edges chosen by our shortest path solution such that they have higher cost than all other edges in our DAG, and solve for a new shortest path. This ensures that these edges will not be chosen again unless they are the only available option. Our second shortest path solution will result in a new set of chosen images, of which we only retain those that cover areas not covered by the first set. This process can be repeated as many times as needed, until holes are no longer present. This method is not as optimal as a 2D-coverage solution would be, but it is a quick approximation, and adequately handles the few holes we run into.

680
681
682
683
684
685
686
687
688
689
With this completed, we have now mapped every location on our plane to at least one image, and have minimized the number of images, as well as the discontinuities between their borders. In the next section, we apply blending between images where they overlap, but for the sake of comparison with the unblended tile caching method in Section 2.2, we arbitrarily choose one image for texturing where images overlap. Figures 3(c) and 3(d) compare the tile caching method against this seam minimization method.

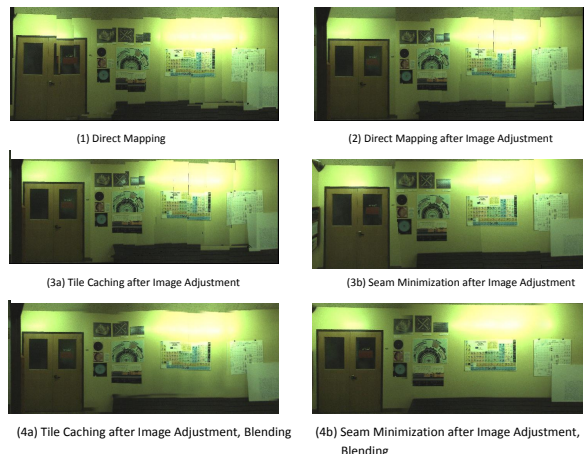
690
691
692
693
694
695
Though both methods provide quite accurate texturing thanks to the alignment process, the seam minimization approach results in fewer visible discontinuities, since it directly reduces the cost of each image boundary, while the tile caching method uses a scoring function that only approximates this effect. Furthermore, seam minimization guarantees the best selection of images, while the sequential tile caching method may select images early on that turn out to be poor choices once subsequent tiles have been processed.

696
697
698
699
700
701
In the context of the backpack modeling system, we apply the seam minimization approach on walls, due to its superior output when provided with head-on images. Floors and ceilings however, given their many images taken at oblique angles, as shown in Figure 6, are textured using the tile caching method.

4.4. Blending

We now apply the same blending process on our two texturing methods: localization refinement followed by either tile caching or seam minimization for texturing.

Although our preprocessing steps and image selections



702
703
704
705
706
707
708
709
710
711
712
713
714
715
716
717
718
719
720
721
722
723
724
725
726
727
728
729
730
731
732
733
734
735
736
737
738
739
740
741
742
743
744
745
746
747
748
749
750
751
752
753
754
755
Figure 8: Textures corresponding to each step in our texture mapping pipeline.

in either method attempt to minimize all mismatches between images, there are sometimes unavoidable discontinuities in our final texture due to different lighting conditions or inaccuracies in planar geometry or projection. These can however be treated and smoothed over by applying alpha blending over image seams. Whether the units we are blending are rectangularly-cropped images or rectangular tiles, we can apply the same blending procedure, as long as we have a guaranteed overlap between units to blend over.

For the tile caching method, we can ensure overlap by texturing a larger tile than needed for display. For example, for a rendered tile $l_1 \times l_1$, we can associate it with a texture $(l_1 + l_2) \times (l_1 + l_2)$ in size. For the seam minimization method, we have already ensured overlap between images. To enforce consistent blending however, we add a minimum required overlap distance while solving the shortest path problem in Section 4.3.2. Additionally, if images overlap in a region greater than the overlap distance, we only apply blending over an area equal to the overlap distance.

After blending pixels linearly across overlapping regions using alpha blending, our texture mapping is complete. Figure 8 shows each incremental step of our texture mapping approach, as well as the final blended output resulting from both of our methods.

5. Results and Conclusions

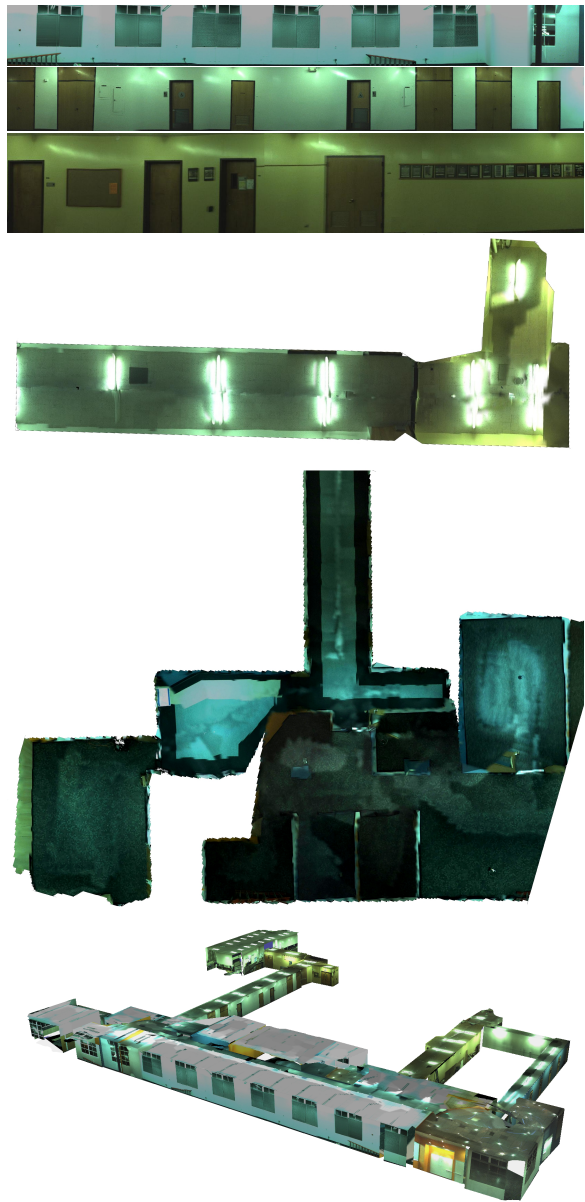
In this paper, we have developed an approach to texture map models with noisy camera localization data. We are able to refine image locations based on feature matching, and robustly handle outliers. We generalized one texture mapping approach to any manner of planes and images, and successfully textured both simple rectangular walls as well as complex floor and ceiling geometry. We also pre-

756
757
758
759
760
761
762
763
764
765
766
767
768
769
770
771
772
773
774
775
776
777
778
779
780
781
782
783
784
785
786
787
788
789
790
791
792
793
794
795
796
797
798
799
800
801
802
803
804
805
806
807
808
809
sented an optimized texturing method that takes advantage
of our localization refinement process and produces more
seamless textures on planes where multiple head-on images
are available. Each of these approaches is highly modular,
and easily tunable for different environments and acquisition
hardware.

Ceilings and floors textured with the tile caching approach, and walls textured with the seam minimization approach, are displayed in Figure 9. High resolution texture comparisons, as well as a walkthrough of a fully textured 3D model are available in the accompanying video to this paper.

References

- [1] M. Brown and D. Lowe. Automatic panoramic image stitching using invariant features. *International Journal of Computer Vision*, 74(1):59–73, 2007. 4
- [2] G. Chen, J. Kua, S. Shum, N. Naikal, M. Carlberg, and A. Zakhor. Indoor localization algorithms for a human-operated backpack system. In *Int. Symp. on 3D Data, Processing, Visualization and Transmission (3DPVT)*. Citeseer, 2010. 1, 2, 3, 4, 5
- [3] E. Dijkstra. A note on two problems in connexion graphs. *Numerische Mathematik*, 1:269–271, 1959. 6
- [4] M. Fischler and R. Bolles. Random sample consensus: a paradigm for model fitting with applications to image analysis and automated cartography. *Communications of the ACM*, 24(6):381–395, 1981. 4
- [5] A. Glassner et al. *An introduction to ray tracing*. Academic Press, 1989. 2
- [6] R. Hartley and A. Zisserman. *Multiple view geometry in computer vision*, volume 2. Cambridge Univ Press, 2000. 1, 4
- [7] J. Kua, N. Corso, and A. Zakhor. Automatic loop closure detection using multiple cameras for 3d indoor localization. In *IS&T/SPIE Electronic Imaging*, 2012. 1, 2
- [8] T. Liu, M. Carlberg, G. Chen, J. Chen, J. Kua, and A. Zakhor. Indoor localization and visualization using a human-operated backpack system. In *Indoor Positioning and Indoor Navigation (IPIN), 2010 International Conference on*, pages 1–10. IEEE, 2010. 1, 2, 4, 5
- [9] D. Lowe. Object recognition from local scale-invariant features. In *Computer Vision, 1999. The Proceedings of the Seventh IEEE International Conference on*, volume 2, pages 1150–1157. Ieee, 1999. 4
- [10] V. Sanchez and A. Zakhor. Planar 3d modeling of building interiors from point cloud data. In *Internation Conference on Image Processing*, 2012. 1



810
811
812
813
814
815
816
817
818
819
820
821
822
823
824
825
826
827
828
829
830
831
832
833
834
835
836
837
838
839
840
841
842
843
844
845
846
847
848
849
850
851
852
853
854
855
856
857
858
859
860
861
862
863
Figure 9: Examples of our final texture mapping output for walls, a ceiling, an entire floor, as well as a fully textured model